LA-4986-MS

AN INFORMAL REPORT

Occurrence of High Energy Electrons and Surface Expansion in Radiantly Heated Target Plasmas

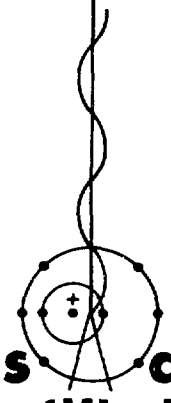

los alamos
scientific laboratory
of the University of California
LOS ALAMOS, NEW MEXICO 87544

UNITED STATES
ATOMIC ENERGY COMMISSION
CONTRACT W-7405-ENG. 36

In the interest of prompt distribution, this LAMS report was not edited by the Technical Information staff.

Printed in the United States of America. Available from
National Technical Information Service
U. S. Department of Commerce
5285 Port Royal Road
Springfield, Virginia 22151
Price: Printed Copy $3.00; Microfiche $0.95

LA-4986-MS
An Informal Report
UC-20
ISSUED: July 1972

los alamos
scientific laboratory
of the University of California
LOS ALAMOS, NEW MEXICO 87544

Occurrence of High Energy Electrons and Surface Expansion in Radiantly Heated Target Plasmas

by

R. L. Morse
C. W. Nielson

OCCURRENCE OF HIGH ENERGY ELECTRONS AND SURFACE EXPANSION IN RADIANTLY HEATED TARGET PLASMAS

by

R. L. Morse and C. W. Nielson

ABSTRACT

It is shown that limitations on collisionless electron thermal conduction place a lower limit on the range of energies of electrons in the surface of target plasmas which are heated by incident electromagnetic radiation, and that in cases of contemporary experimental interest these energies can be hundreds of keV. It is then shown that these high energy electrons can cause a much faster expansion of plasma from the heated surface than would be predicted by a single fluid theory. Numerical simulations demonstrate both effects.

I. INTRODUCTION

When electromagnetic radiation is absorbed in the surface of a fully ionized plasma most of the absorbed radiation energy is deposited in the form of electron kinetic energy. If the power density of the incident radiation is sufficiently great the plasma may be assumed to be approximately collisionless, which means that the important absorption mechanisms may be collective and that there is no reason to expect the velocity distribution of the heated electrons to be even approximately Maxwellian.[1] The purposes of this paper are to show, first, that in some cases of experimental interest the absorbed energy should be expected to come to reside uniformly throughout the target plasma in a very non-Maxwellian low density, high temperature tail of the electron velocity distribution, and, second, that this highly non-equilibrium electron distribution can cause its energy to be lost, through a low density, high velocity expansion of the plasma surface ("blow off"), much faster than energy would be lost by a simple, single temperature fluid expansion.

II. ABSORPTION AND COLLISIONLESS THERMAL CONDUCTION

Here we will not consider the many absorption mechanisms in detail, but will instead group them into two classes according to their statistical properties. Absorption in the surface region of a plasma, the main body of which is over dense, i.e., which has a plasma frequency higher than the incident wave frequency, occurs in layers of restricted thickness, usually at or near the critical surface where the wave and local plasma frequencies are equal. In this absorption or heating region an average electron may receive the final velocity with which it leaves the region from a large number of small, almost random impulses of roughly equal magnitude. In such cases we will say that the absorption region is stochastically thick. This condition will occur in some cases in which electrons are heated by a broad spectrum of electric field fluctuations caused by the development of a plasma instability. It also occurs when electrons are heated by multiple binary collisions with ions, which is sometimes called inverse bremsstrahlung. Although it has been observed that when incident power densities are high enough to heat target plasmas to thermonuclear temperatures the plasma temperature in the absorbing region is often so high

that collisional absorption is ineffective in hydrogen, collisional absorption could be sufficiently enhanced to be effective by the inclusion of higher Z (ion charge) materials in the absorbing region. In this case, however, the subsequent transport of electron energy out of the absorbing region would be more nearly collision dominated and some of the electron energies involved would necessarily be even higher than those estimated below by collisionless arguments.

If on the other hand, the statistical distribution of impulses is such that an average electron receives only one relatively large impulse while it is in the absorption or heating region then we will say that the region is stochastically thin. This condition occurs in particular when the absorption is caused by resonance or radiation pressure.[2]

At the power densities of interest here these heated electrons leave the absorption region with velocities which are much higher than the initial mean thermal velocity of the other plasma electrons. The electron velocity distribution which develops near, but outside of the heating region has been seen from numerical simulations (see Appendix) to consist of a broad, nearly flat component of energetic electrons streaming from the heating region into the main body of the plasma and a cold background component of electrons counter streaming into the heating region. (This is quite different from the velocity distributions associated with weaker, collision dominated thermal conduction, which are nearly Maxwellian but slightly skewed to acquire a non-zero third moment.) For now in modeling this collisionless thermal conduction we adhere to a strictly one dimensional picture of the energy deposition and conduction process. The coordinate x runs normal to the plasma surface. All quantities are independent of y and z. A net flow of energy goes in the positive x direction. Later we will comment on consequences of relaxing the one dimensionality. The crucial issue here is the form of the electron velocity distribution when it is constrained by the requirements that it should not support beam plasma instabilities and that it should represent zero current flow, i.e., $J_x = 0$, in order to preserve charge balance. Here we ask what distribution has the smallest value of maximum electron energy, consistent with a given energy flux, Q. According to the standard definition

$$Q = \frac{m_e}{2} \int_{-\infty}^{\infty} dv_x v_x^3 f(v_x) \qquad (1)$$

where $f(v_x)$ is the electron velocity distribution. It is tempting to choose the form of $f(v_x)$ sketched in Fig. 1a, which represents an energy flux in the positive x direction while the essentially delta function cold electron distribution streams back into the heating region with the necessary negative

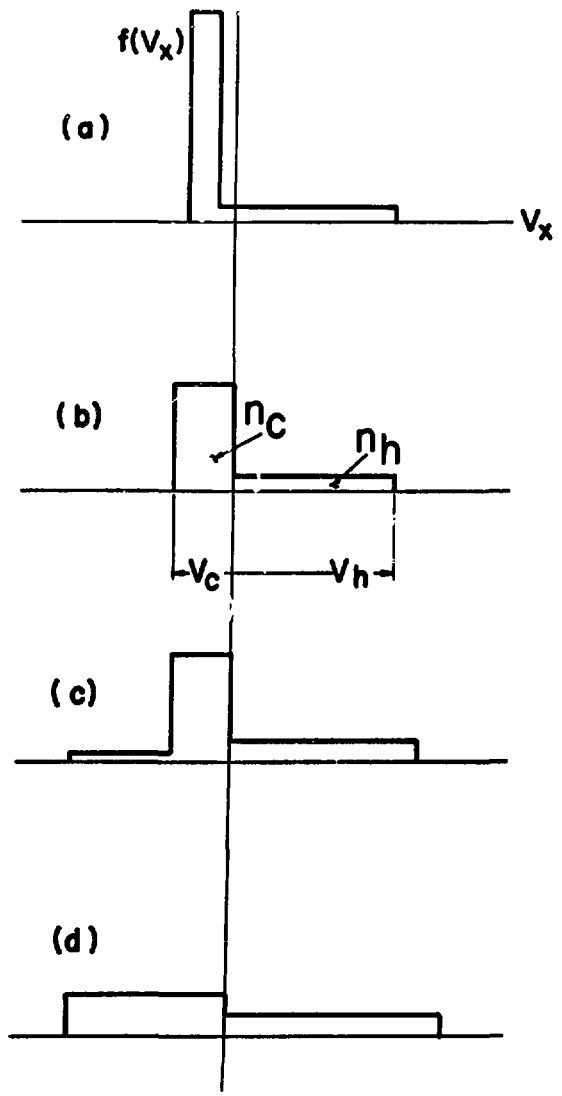

Fig. 1. Energy conducting velocity distributions (a) without thermal broadening of cold counterstreaming electrons, (b) with instability broadening of cold electrons, (c) with returning hot electrons and (d) when hot electrons have completely excluded cold electrons from the heating region.

velocity to give $J_x = 0$. This distribution has only a single maximum and is therefore stable to beam instabilities within itself. However, simulations of this collisionless heat conduction process, which are presented in the Appendix, show that the interaction between the heated electrons and the counterstreaming cold background electrons broadens the velocity distribution of the latter to the point where Fig. 1b is a better description of $f(v_x)$. Moreover, when ion motion is included in the process and the ions are initially cold the development of the more slowly growing ion acoustic instability between the ions and the cold electrons[3] forces the cold electron velocity distribution to be broadened by more than enough to include the ion velocity, which is zero here, as shown in detail in Ref. 4. This makes the requirement for hot electrons even a little stronger than we derive here. Hence, we are led to the idealized form (Fig. 1b)

$$f(v_x) = \begin{cases} n_h / v_h , & 0 < v_x < v_h \\ n_c / v_c , & -v_c < v_x < 0 \end{cases} . \qquad (2)$$

In order that J_x be zero the hot and cold components are related by

$$J_x = \int_{-\infty}^{\infty} dv_x v_x f(v_x) = \tfrac{1}{2}(n_h v_h - n_c v_c) = 0 \qquad (3)$$

or

$$v_c = \frac{n_h}{n_c} v_h \qquad (4)$$

and from Eq. (1)

$$Q = \frac{n m v_h^3}{2} \left\{ \frac{n_h}{4n} \left[1 - \left(\frac{n_h}{n - n_h} \right)^2 \right] \right\} \qquad (5)$$

where $n = n_h + n_c$. Figure 2 shows $Q/(n m v_h^3/2)$ as a function of n_h/n, from which we see the simple but important result that for a given Q there is a minimum value of v_h, $v_{h\,min}$, given by

$$\frac{Q}{\left(\frac{n m v_h^3}{2} \right)_{min}} = \frac{1}{16} = 0.0625 \qquad (6)$$

which is achieved when $n_h/n = 1/3$. This appears to give about the largest Q that can be obtained with a given effective limit, v_h, on the velocity of the energetic electrons. It is interesting to note in passing that one sometimes encounters "back of the envelope" estimates in which 1.0 or 0.5 is used in place of 0.0625 on the right side of Eq. (6), and this of course seriously over estimates Q or under estimates v_h.

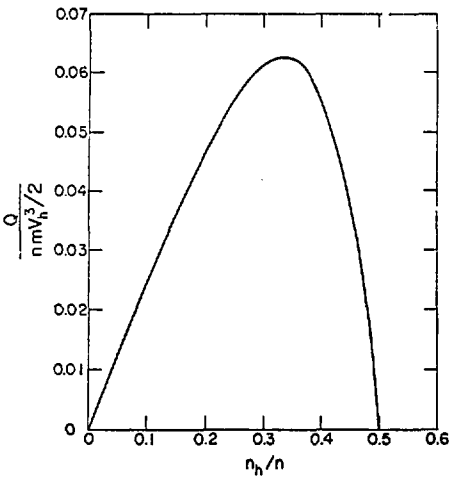

Fig. 2. Energy flux, Q, as a function of the ratio n_h/n of hot electrons to total electron density for the velocity distribution in Fig. 1b.

As the numerical simulations show, stochastically thick absorption establishes the same electron velocity distribution with v_h close to $v_{h\,min}$ for a given v_h, regardless of the details of the absorption mechanism. Hence, an example based on this optimum is physically interesting. Suppose that an absorbed power density, i.e., Q, of 10^{17} W/cm^2 is to be transported in from a plasma surface through the density of solid hydrogen, $n \simeq 3 \times 10^{22}$ cm^{-3}. Then Eq. (6) gives $v_{h\,min} \simeq 0.95 \times 10^{10}$ cm/sec, which corresponds to a maximum electron energy of about 25 keV. If, on the other hand, this energy were deposited at the critical density of $n = 10^{21}$, belonging to the 1.06 μ light from N_d^{3+}, then the maximum electron energy would be about 340 keV. If the energy is deposited at the still lower critical density of $n = 10^{19}$ for the 10.6 μ light from CO_2 then the resulting electron energies are so large that a relativistic treatment is required. Alternatively, 10.6 μ light would produce 340 keV electrons from a power density of only 10^{15} W/cm^2. These large electron energies should be thought of as a consequence of the perhaps surprisingly limited ability of physically attainable velocity distributions to transport energy out of the heating region.

It is noteworthy that the electron energies predicted on this basis are in all non-relativistic cases much larger than the driven energy of oscillation of an electron in an incident wave field

with a power density equal to the absorbed power density. For example 10^{17} W/cm^2 at $\lambda = 1.06\ \mu$ drives an electron to about 25 keV, in contrast with the 340 keV obtained above. Likewise for 10^{15} W/cm^2 at $\lambda = 10.6\ \mu$ since both driven and transport determined energies are functions of Q/n. Since some plasma instabilities, as well as binary collisions, are greatly depressed by thermal energies well above the oscillating energy, the efficiency of these absorption mechanisms may be limited by the inability of electron transport to remove energy from the heating region.

If the absorption region is not stochastically thick then in principle v_h can be much larger than $v_{h\ min}$ and n_h/n will in general be less than the optimum value of 1/3. Collisionless thermal transport velocity distributions of the kind idealized in Fig. 1b are seen in the numerical simulation (see Appendix) of the thin, resonant absorption process. These parameters place the conduction process on the left end of the curve in Fig. 2. As shown in Ref. [2] there are indeed thin absorption processes which are capable of producing electron energies considerably larger than $(nmv^2_{h\ min}/2)$. These may be particularly significant when absorption occurs at near solid densities where the electron energies produced by thick absorption are not very large.

As the heated electrons move away from the absorption region and into the main body of the plasma where the density is higher their energies are only slightly reduced (less than 1% for the more energetic electrons when $n_h/n = 1/3$) by self-consistent electrostatic fields as is easily confirmed by keeping Q and $f_h = n_h/v_h$ fixed while passing to the limit $n_h/n \to 0$ in Eqs. (3)-(5).

If the dimensions of the target are of the order of or large compared with the collisional mean free path of the energetic electrons, then the effect of these electrons will be to deposit the absorbed energy more deeply into the target or to a given depth in a shorter time than would be done by diffusion of thermal electrons. In cases where deposition of the absorbed energy in the greatest mass of target material is desired this may be helpful. For example the mean free path of 100 keV electrons in a cold hydrogen plasma with the solid density of 5×10^{22} cm^{-3} is about 0.5 cm. The mean free path is, of course, shorter in higher Z (ion charge) plasmas with the same electron density, a fact which could be used to reduce electron range, if that were desired, by doping targets with high Z materials. At the same time, however, inclusion of high Z material in the target plasma does increase the re-radiation energy loss by bremstrahlung.

If, on the other hand, the target plasma is bounded by dimensions which are much smaller than the energetic electron mean free paths, then these electrons will distribute themselves throughout the target in a few transit times and establish the spatially uniform low density distribution of hot electrons referred to in the introduction. Only when the absorption is thick and occurs at a density not much less than that of the main body of the plasma will the hot electron density not be much less than the cold, and in many cases of interest the heated electrons are then collision dominated so that these considerations do not apply correctly. If the heating pulse duration is longer than the time of transit of the energetic electrons across a bounded target then these electrons will return to participate in the heating process more than once. If, for example, the heating pulse lasts one nano sec and the bounding dimensions of the target are one millimeter then a three hundred kilovolt electron would return to the heating region many times, especially if the heating region extends over a significant fraction of the target surface area. At first the returning energetic electrons modify the velocity distribution shown in Fig. 1b to the (equally idealized) form shown in Fig. 1c with smaller value of f(v) in the returning electron tail ($v < 0$), than in that part of f(v) leaving the heating region, ($v > 0$), which reflects the usual condition that the absorption does not occur uniformly over the entire target surface. When the density of hot electrons in the main body of the plasma has increased to the total electron density in the heating region (usually the critical density) then the cold electrons are altogether excluded from the heating region because, as we discuss below in connection with surface expansion, the cold electrons are in a sense infinitely polarizable. The electron velocity distribution adjacent to the heating region then acquires

the form sketched in Fig. 1d. From this point on no additional cold electrons are heated in the heating region except as a result of overall expansion of the target. Instead the hot electrons are heated further if the absorption continues. These phenomena can be seen in numerical simulations like those in the Appendix but carried further in time and with a density gradient.

An important point is that if absorption goes on much longer than a target transit time, depending on how thick the absorption is, the density of the energetic electrons rises to just the density at the absorption region which means, as we shall show below, that expansion causes a step in density to occur at that point.

There are several respects in which our one dimensional, collisionless treatment would need to be improved in order to make good quantitative predictions of target behavior. First, if we allow electron motions in y and z then the effective specific heat of the electrons transporting energy out of the absorption region can be increased. Hence Q can be larger for a given v_h, depending on the magnitude of the thermal spread in v_y and v_z, and thus on the degree of anisotropy of velocities developed in the absorption region. Instability and collisional absorption tend to produce a relatively isotropic velocity distribution, but the resonant and radiation pressure mechanisms do accelerate electrons primarily normal to the local target surface. However, large velocity anisotropies may not be tolerated by instabilities of the Weibel[5] type, which has been shown by simulation to decrease, and in many cases essentially eliminate, electron velocity anisotropy.[6] The effect of isotropic distributions of electron velocities is to increase Q by as much as about 3 for a given v_h, or the maximum electron energy by about 2 for a given Q, which is not enough to change the basic qualitative conclusions reached here. The two or three dimensional development of the electrostatic instabilities, which are shown in the appendix to be caused by counter streaming between heated and cold electrons, is expected to be, if anything, weaker than in the one dimensional treatment there, on the basis of previous simulations.[7]

If the energy absorption is localized to a spot on the target surface then a multidimensional treatment of the heat transport can be expected to introduce circulating thermo-electric currents since it does not necessarily follow that the flux of the hot electrons and the charge compensating counter flow of cold electrons will be co-linear. This current flow, together with the self consistent magnetic fields cannot be calculated properly without a multi-dimensional simulation.

Another point of realism is that even though the hot electrons may be quite accurately regarded as collisionless, the counter streaming cold electrons may not, particularly early in time when the electrons in the main body of the plasma have not yet been sufficiently heated. Hence, in some cases there will be a need to include the effective electrical resistivity of the cold electrons flowing through the ion background, to calculate the E field necessary to drive the required current, and to modify the hot electron trajectories with this field. This of course is the first step back toward collisional thermal conductivity.

Finally, at the very beginning of the heating process the main body of the target need not even by ionized. In this event the hot electrons cannot leave the heating region at first because no cold but free electrons are available to compensate their loss. Eventually, of course, collisional thermal conduction will cause the necessary ionization, but on a faster time scale the hot electrons can protrude into the un-ionized region by their Debye length, which can be large, and cause ionization and heating. Here we only speculate that this burn through process may be important in some cases of interest.

III. HIGH VELOCITY, LOW DENSITY SURFACE EXPANSION

In this section we begin with a bounded plasma consisting of three components: cold ions at a density n_i, cold electrons at a density n_c and hot electrons at a temperature T_h and a density n_h, such that $n_c + n_h = n_e$, $= n_i z$; that is we assume quasi neutrality and $n_h \ll n_c$ in the main body of

the plasma. In practice of course the cold electrons must have some temperature but by cold we mean here that this temperature is sufficiently low that the cold electron pressure is much less than the hot electron pressure. Finite cold electron pressure would cause an additional lower velocity, higher density expansion. We shall assume that the hot electrons have a Maxwellian velocity distribution. This is a bit arbitrary as we can see from the electron transport studies above, but is convenient and as representative as any other distribution that we could choose. The mass motion of the ions will be taken to be sufficiently slow that the electron distribution is always in a stationary state. Since cold electrons are in a sense infinitely polarisable, cold electrons are everywhere except at the edges of the plasma where the total electron density, n_e, drops below n_{ho}, and the cold electrons are totally excluded.

If we consider a half space problem in which there is a uniform plasma where $x \to -\infty$ and vacuum where $x \to +\infty$, all of which is independent of y and z then an expansion of the surface in the x direction does not modify the original Maxwellian velocity distribution of the hot electrons and their density in the low density region is

$$n_h = n_{ho} \exp\left[\frac{-e\varphi(x)}{kT_h}\right] = zn_i, \quad \text{where } kT_h = \frac{m_e v_h^2}{2} \qquad (7)$$

In practice then, since we are really interested in bounded targets we are only following the early phase of the expansion before it significantly increases the effective volume occupied by the hot electrons. We assume that at time t = 0 the total density also has a uniform value, n_{eo}, for $x < 0$ and is zero for $x > 0$. An initial density gradient at the surface as in Ref. 2 will not change the basic result. The following two step expansion then occurs at the surface.

First, an abrupt step in φ develops from $\varphi = 0$ to $\varphi = \varphi_1 < 0$ right at x = 0, which accelerates ions from rest to a velocity $v_1 > 0$. By energy conservation $Ze\varphi = m_i v_1^2/2$. Actually if the step in φ stands fixed at x = 0, while ions stream through, then ions must have a velocity v_o at $x < 0$, but, as will be clear from the following derivation, when $n_{ho} \ll n_c$ then v_o^2 is much less than v_1^2 and can be neglected. Just to the right of the step the cold electrons are excluded because the total density, n_e, is less than n_{ho}, and from Eq. (7) the density of hot electrons is

$$n_{h1} = n_{ho} \exp\left[\frac{-e\varphi}{kT_h}\right] = n_{ho} \exp\left[\frac{-m_i v_1^2}{2kT_h}\right] \qquad (8)$$

The equation expressing pressure and momentum balance across the step is then

$$n_h kT_h = n_{h1} kT_h + n_{h1} \frac{m_i v_1^2}{Z}, \qquad (9)$$

where again terms proportional to v_o have been dropped. Substituting from Eq. (8) into Eq. (9) gives

$$1 = \left(1 + \frac{m_i v_1^2}{ZkT_h}\right) \exp\left[\frac{-m_i v_1^2}{2ZkT_h}\right], \qquad (10)$$

a transcendental equation with the solution

$$\frac{m_i v_1^2}{ZkT_h} \simeq 2.5, \quad \frac{n_{h1}}{n_{ho}} \simeq 0.29 \text{ and } \frac{v_1}{c_h} \simeq 1.58 . \qquad (11)$$

where $c_h = ZkT_h/m_i$, the ion acoustic velocity calculated from the hot electron temperature alone. The thickness of the step derived here would be of the order of a Debye length if charge separation were included in the treatment. We see that $n_{h1} < n_{ho}$, which justifies exclusion of the cold electrons to the right of the step and gives a sufficiently low mass flow rate through the step to make $v_o \ll v_1$ if $n_{ho} \ll n_c$. We see also that v_1 is much larger than the acoustic speed calculated from the average temperature, $T_h n_{ho}/(n_{ho} + n_c)$.

Once through the step the ions then continue to accelerate as a function of time and position as in a conventional isothermal rarefaction in the rest frame moving with the velocity $(v_1 - c_h)$. The ion velocity is, therefore, given by

$$v_i = v_1 + x/t \qquad (12)$$

and the density is given by

$$n_e = zn_i = n_{h1} \exp\left[\frac{-x}{tc_h}\right] \qquad (13)$$

The total ion energy is

$$\mathcal{E}_i = \int_o^\infty dx \frac{n_i m_i v_i^2}{2} = \frac{n_{h1} m_i}{2Z} \int_o^\infty dx \,(v_1 + \frac{x}{t})^2 \exp\left[\frac{-x}{tc_h}\right]$$

$$= \frac{n_{h1} m_i c_h^3 t}{2Z} \times \left[\left(\frac{v_1}{c_h}\right)^2 + 2\left(\frac{v_1}{c_h}\right) + 2\right]. \qquad (14)$$

Substituting from Eqs. (11) for n_{hl} and v_1 gives

$$\mathcal{E}_1 \simeq 0.46 \frac{n_{ho} m_i c_h^3 t}{2Z} \qquad (15)$$

$$= 0.153\, c_h t \left(\frac{3 n_{ho} k T_h}{2}\right)$$

where

$$c_h = \sqrt{\frac{ZkT_h}{m_i}}$$

Since the energy density in the plasma is $(3/2)n_{ho}kT_h$, the basic result is that when $0.153\, c_h t$ approaches the size of the system then the effective volume containing the hot electrons has increased by approximately two, four or eight depending on symmetry (plane, cylindrical or spherical) and the hot electron energy has been substantially dissipated by the low density, high velocity blow off. Experimentally the energy would appear in the form of ions moving away from the surface with energies of the order of and larger than Z times the mean hot electron energy.

If the surface density gradient which exists when the hot electrons appear is sufficiently gradual that the length interval from the vacuum to the point where $n_e = n_{ho}$ is substantially greater than the hot electron Debye length thickness of the step in φ, then at first all of the ions in this interval will be accelerated by the gradient of φ which follows from Eq. (8) above. This is the behavior which is beginning to occur in Fig. 4 of Ref. 2. When these ions have moved off enough to drop the density in this interval below n_{hl}, then the step will establish itself where $n_e = n_{ho}$ and begin to eat its way back into higher density region as more ions pass through the step. When the electron density on the high density side of the step is just n_{ho} then the ion velocity on the high density side, which we neglected above is $v_o = (n_{hl}/n_{ho})v_1 = 0.29\, v_1$ which is not negligible but not large enough to make any qualitative change if it were included in Eqs. (8) and (9).

When the density of energetic electrons has not yet exceeded the absorption region density then the blow off step begins on the low density side, as seen clearly in Fig. 4 of Ref. 2. However, as discussed above if the absorption goes on for much longer than a target transit time the hot electron density, n_{ho}, can rise up to but not above the density in the heating region. This then causes the step to occur right in the heating region. As the step progresses into the higher density region the density on its high side will increase above n_{ho} while the density on the low side will remain $n_{hl} \simeq 0.29\, n_{ho}$. Thus at least when there is a particular absorption density or narrow range of densities, this absorption density would be found only in the step, a situation which would modify the absorption process by reducing the thickness of the absorption region. As collisions with the hot electrons build up the cold electron pressure, however, this pressure will broaden the step somewhat as it works to cause the second lower velocity rarefaction.

In the section on electron heating above we pointed out that the increased range of energetic electrons could help in depositing absorbed energy in a thicker surface layer of material. This is important when one wishes to deliver the maximum possible recoil impulse to the surface, from expansion of surface material, for a given absorbed energy. On the other hand it is very important for some applications to note that when in a bounded target the high energy electrons and low density blow off occur, much less mass is blown off than in a simple fluid expansion. The absorbed energy is, therefore, used much less efficiently in imparting impulse to the surface. If the bounded target is homogeneous so that the hot electron distribution does indeed extend uniformly throughout the target then the situation is even worse because the expansion recoil on one side of the target balances that on the other side without giving any impulse at all to the bulk of the target.

From Eq. (15) it can be seen that the rate of energy loss by expansion can be reduced by making the ratio m_i/Z_i large, which can be accomplished in principle by using high Z materials so that m_i is large, but in a low ionization state so that Z_i is effectively small.

IV. NUMERICAL SIMULATION OF THE LOW DENSITY, HIGH VELOCITY SURFACE EXPANSION

The following one dimensional, electrostatic, Particle-In-Cell[8] simulation shows the low density surface expansion more graphically than the above analytic derivation and gives us confidence in predicting the effect. Figure 3a shows the initial

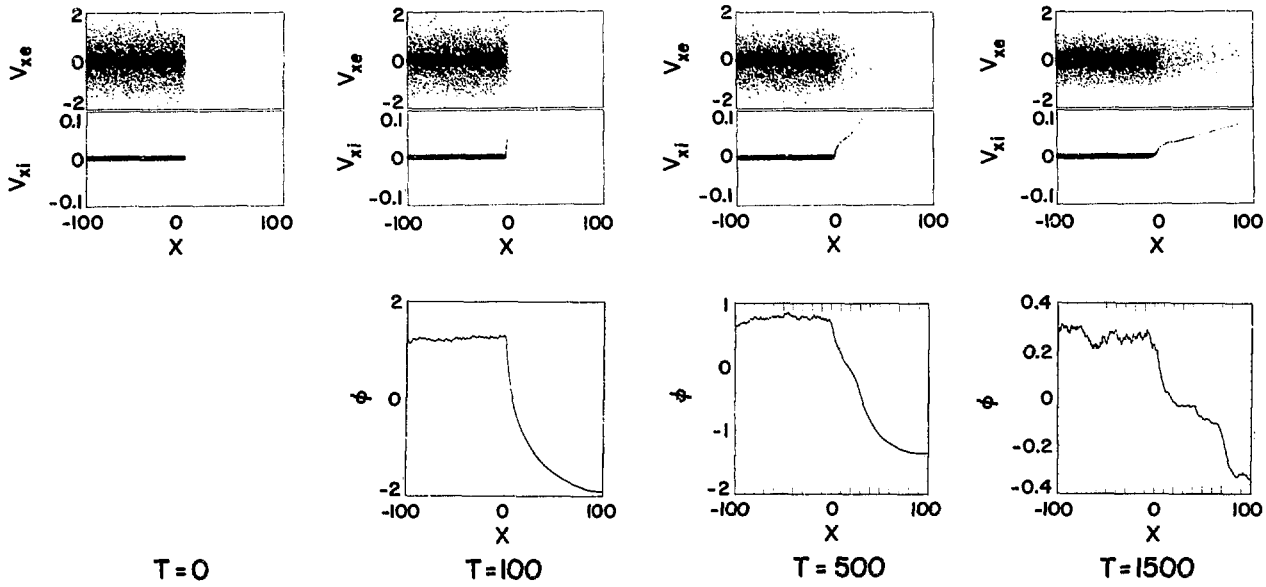

Fig. 3. Phase space plots of hot and cold electrons (above) and ions (below) and accompanying graphs of $\varphi(x)$ at (a) initial time, t= 0, (b) t = 100 when ion motion has just begun at x = 0, (c) t = 500 when the formation of the step in ion velocity and $\varphi(x)$ has developed and the expansion-rarefaction motion of ions has begun and (d) t = 1500 when the expansion is well developed and considerable cooling of the hot electrons has occurred.

phase space plots, v_x vs x, of electrons (above) and ions (below). The ion to electron mass ratio is 1000, an arbitrary number chosen large enough that the electrons have an almost stationary velocity distribution almost everywhere, and Z = 1. Particles which reach the grid boundaries are reflected. The grid has a length of 200 Debye lengths based on the total electron density and the thermal velocity, v_h = 1.0, of the hot electrons. The initial ratio of hot to cold electron densities, n_{ho}/n_c, is everywhere 0.1. The cold electrons initially have a small thermal spread of 0.05, which is necessary to prevent a small Debye length numerical instability which gives some energy to the cold electrons whether you like it or not if their Debye length is smaller than the cell size. It was also found to be helpful to represent the cold electrons with simulation particles each of which represent ten times more electrons than are represented by the hot electron simulation particles, in order to improve hot particle statistics. Time units are ω_{pe}^{-1}. Figure 3b shows the phase plots and the electrostatic potential, $\varphi(x)$, at t = 100, just as the step is beginning to form. Note that the hot electrons have begun to protrude out into the vacuum (the Debye length of the hot electrons is much longer than that of the cold), the ions at the surface have begun to accelerate and the potential is essentially flat where there are cold electrons, in keeping with their large polarisability. Figure 3c shows the same combination of diagnostics at t = 500 when the ion phase plot shows the beginning of the low density expansion from the top of the step in ion velocity. From Eq. (11) the velocity v_1 at which the step breaks over into the rarefaction should be $1.58 \times \sqrt{1/(2 \times 10^3)} = 0.033$ in the units of the simulation, and this is what is seen here to within the accuracy with which one can identify this velocity from Fig. 3c. Also the slope of the rarefaction line in phase space beyond the step agrees with Eq. (12), and the ion density profile (not shown here) is in full agreement with the analytic model, Eq. (13). Figure 3d shows the situation at t = 1500 when the expansion is well developed and a large fraction of the original hot electron energy has gone into the expanding ions. This is reflected in the fact that the step velocity at x = 0, v_1, is now noticeably smaller than in Fig. 3c.

V. CONCLUSIONS

We have examined the process of collisionless thermal conduction out of a region where energy is deposited by absorption of electromagnetic radiation and found lower limits on the top of the range of energies of electrons involved in the process. These lower limits, given approximately by Eq. (6) above, depend only on the rate of energy absorption and the electron density at which it is absorbed, and not at all on the details of the absorption process. From absorption of 10^{15} W/cm^2 at the critical electron density of 10^{19} cm^{-3} of 10.6 μ light, electron energies up to 390 keV must occur. The same energies must occur from the absorption of 10^{17} W/cm^2 at the critical density of 10^{21} cm^{-3} of 1.06 μ light, because of the inverse relationship between power and density in Eq. (6). Such energetic electrons have mean free paths of centimeters in hydrogen plasmas with solid densities. Consequently long lived two temperature velocity distributions can be expected from such power inputs into bounded target with dimensions of the order of a millimeter or less. In general the high energy electrons from the surface are expected to distribute themselves throughout the available target volume with a density not greater than the electron density at the point in the surface where they are heated, and, therefore, in most cases, at a much lower density than the rest of the colder electrons in the main body of the target. This can be advantageous if a uniform distribution of electron pressure in the target is desired. The use of high Z materials in the target is recommended to reduce the lifetime and range of these high energy electrons if this is desired.

As a further consequence of the occurrence of the two temperature electron distribution, a low density surface expansion and rarefaction is predicted with expanding ions accelerated to energies greater than the mean energy of the high temperature electrons. This expansion is capable of dissipating the hot electron energy much faster than would be done by a conventional hydrodynamic expansion, while giving relatively little recoil impulse to the target surface. This low density, high velocity expansion would be moderated by the presence in the surface of high Z, weakly ionized material.

APPENDIX

The following numerical simulations were done by the Particle-In-Cell (P.I.C.) method[8] on a one dimensional grid. The electrons move under the influence of the self consistent electrostatic field obtained on each time step from Poisson's equation, and are represented by 8×10^4 simulation particles. The ions are represented by a fixed, uniform positive charge background. At the left boundary, $x = 0$, the electric field, $E_x = d\varphi/dx$, is set to zero, and at the right end, $x = 800$ for all of the simulations shown here, the potential, φ, is zero. The units of time are ω_{pe}^{-1}, and the units of length are v_o/ω_{pe}, where v_o is the velocity unit of the simulations, and therefore the unit of velocity in which the graphs below are labeled. If the electron velocity distribution had the form $f(v_x) \sim \exp[-v_x^2/v_o^2]$ then $v_o/(\sqrt{2}\omega_{pe})$ would be the Debye length. In these units the time step and cell length used were both 0.2, giving a total of 4×10^3 cells in the grid length of 800. There are two kinds of problems, those in which heat enters the system and those in which it leaves. Both situations have been simulated. Here we present the "heat entering" results, and only comment on the others below. The simulations are started with the grid filled uniformly by a Maxwellian distribution of electrons with a thermal velocity spread of 0.05, which is very small in comparison with eventual velocities. Particle motions are reflected from both ends of the grid as they would be by space charge sheaths in a real slab target. The energy is introduced into the left end of the grid in the following way. A heating or energy deposition region is chosen, essentially arbitrarily, but in order to avoid numerical truncation errors it should be long enough that a heated particle does not leave the region in one time step. In all the simulations presented here this interval, whose length we call h, was $x = 0$ to 10, so $h = 10$, although in earlier work this length was varied widely as an alternative

way of varying the effective stochastic thickness of the heating region. On each time step each particle in the region is given a velocity increment or impulse chosen randomly from a distribution. This distribution can be almost arbitrary, particularly in thick heating regions where the central limit theorem guarantees that almost all such distributions of individual impulses will tend to build up a Maxwellian velocity distribution. Reduced heating of more energetic electrons because collision cross section dependence on velocity or band limits of plasma turbulence are included in this approximation by reducing the mean magnitude of these impulses for more energetic electrons, but such effects were not included in the calculations presented here. Here the impulse distribution was specified by first making a random selection on each time step of some fraction, F, of the particles in the heating region. Each of the selected particles is then given an impulse, δv_x, chosen randomly from the interval $\delta v_x < \delta v_x < \delta v_{max}$ (a flat topped distribution of δv_x's); the remainder of the particles are given $\delta v_x = 0$. Then because this distribution of δv_x's is symmetric the average energy increment per particle in the heating region per time step in $Fm\langle \delta v_x \rangle/2 = Fm\delta v_{max}^2/6$. Thus the energy flux into the grid is

$$Q = (nh\ F\ \delta v_{max}^2)/(6\Delta t) \qquad (A1)$$

where n is the density of simulation particles and we have set m = 1 as is done for electrons in the simulations. Here we are making no effort to put Q into physical units since the desired results are dimensionless ratios. In the same units the energy flux at any point in the grid is

$$Q = \frac{n\langle v_x^3 \rangle}{2} . \qquad (A2)$$

In all of the simulations presented here h = 10 and $\Delta t = 0.2$, and the parameters giver above make n = 100 simulation particles per unit length.

CASE I

In this first case F = 1, i.e., all particles receive an impulse on each time step, and $\delta v_{max} = 0.1$ so that from Eq. (A1) $Q = 50/6 \simeq 8.33$ and from setting the right sides of A1 and A2 equal the steady state value of $\langle v_x^3 \rangle$ coming out of the heating region should be $\langle v_x^3 \rangle = 1/6 \simeq 0.166$. These parameters are such that an average electron will acquire a velocity of the order of one from of the order of 10^2 impulses. Hence in the sense described in the test this heating region is clearly stochastically thick. Figure A-1 shows the phase

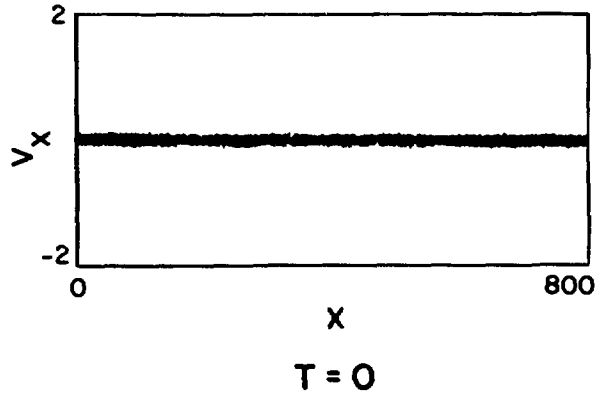

Fig. A-1. Phase plot of electrons at initial time in the simulation of collisionless thermal conduction

space of Case I at zero time. Fig. A-2 at t = 160 shows the phase space and the potential, $\varphi(x)$, at t = 160. At this early time it is easiest to see the dominant physical phenomena involved in collisionless energy transport. Heated electrons stream out of the heating region to the right and create a charge separation potential difference which draws adjacent cold electrons back into the heating region to neutralize the charge imbalance. This is seen in Fig. A-2 in the potential maximum at the left end of the grid (the electrons are treated as negatively charged) and the downward shift of the main strip of cold electrons to negative velocities in this same region of the phase plot. The large oscillations of $\varphi(x)$ are not numerical noise (as are some of the fluctuations of the velocity moments shown below) but rather electrostatic oscillations caused by counterstreaming between the faster heated electrons, which escape the heating region first, and the cold electrons. The wavelength of these oscillations, which is between 5 and 10 here, is a bit difficult to resolve with

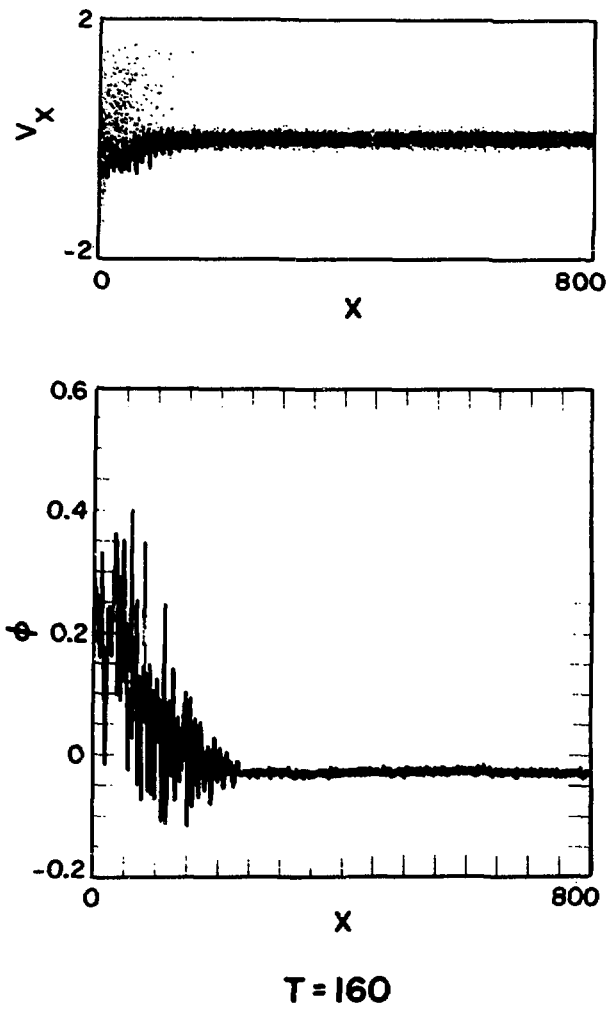

Fig. A-2. The phase plot of electrons and the electrostatic potential early in Case I, the stochastically thick absorption case, show the beginning of cold electron counterstreaming and the associated gross structure of $\phi(x)$ and v_x associated with the counter-streaming instability.

the eye in Fig. A-2 but is adequately resolved by the 4×10^3 cells of length 0.2. Because the faster heated electrons move further into the cold region sooner they establish a bump on tail velocity distribution which is unstable to the growth of plasma oscillations, which in turn causes[3] some slowing and spreading of velocities and persist in time because they are weakly damped. These plasma oscillations can also be seen in the short wavelength oscillations of the cold electrons in the phase space plot. The bump on tail problem is treated in detail for a homogeneous plasma in Ref. 8, in which Case IV most closely resembles the two beam situation seen here. The shift of the peak of an energy conducting electron velocity distribution away from the local ion rest frame tends also to cause the more slowly growing ion acoustic instability, as has been pointed out by Forslund[3] especially when the ions are colder than the electrons. In the situation under study here this is essentially an unstable interaction between the ions and the cold, counterstreaming electrons, and is stabilized when the thermal velocity spread of the latter is of the order of their drift velocity with respect to the ions. A flat spot also develops in the electron distribution at the zero, or ion, velocity. This has been seen in other simulations of the kind shown here but with ion motion included and was shown previously in numerical simulations of ion acoustic turbulence.[4] This additional heating of the cold electrons has been seen in simulations with the hydrogen mass ratio to make the overall electron velocity distribution significantly more nearly bell shaped, and thus further strengthen the need for hot electrons to transport a given Q. The details depend on the mass ratio and the initial ion temperature, the effect being stronger of course with colder ions. Besides, as we see in Figs. A-3 and A-4 the interaction of hot and cold electrons has already caused almost this much heating of the cold electrons.

Before continuing with the simulations of the energy transport we would like to note that several other cases have been run with values of the heating region parameters, h, F and δv_{max}, which ranged widely but were constrained to give stochastically thick heating and the same value of $\langle v_x^3 \rangle$, 0.166, by Eq. (A-1). Predictably the results were virtually identical outside of the heating region, because the same almost Maxwellian velocity distribution develops inside the heating region. This independence of the details of energy transport from the microscopic details of all thick energy deposition processes would seem to make a broad class of plasma turbulence collisional absorption mech-

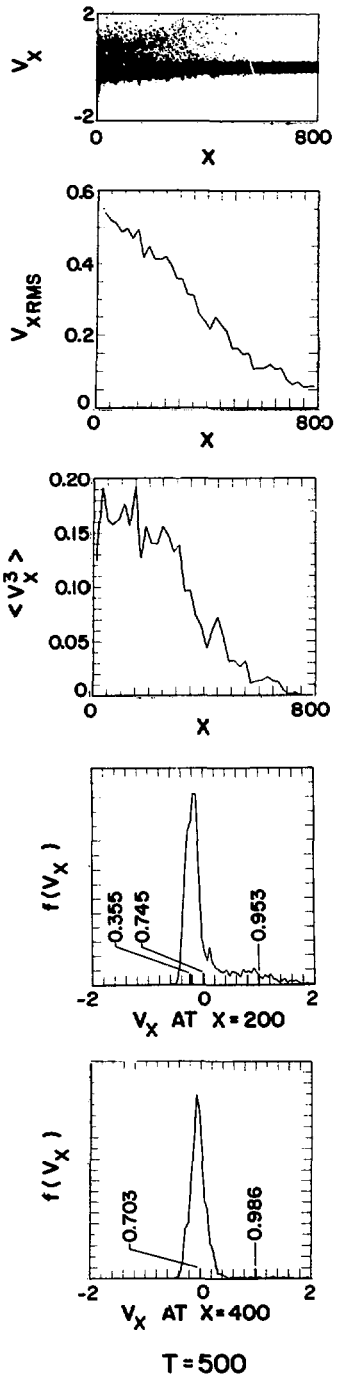

Fig. A-3. Electron phase plot, graphs of mean thermal velocity spread, Vrms, the thermal conduction moment, $\langle v_x^3 \rangle$, and the velocity distributions at x = 200 and 400, taken at t = 500 ω_{pe}^{-1} from Case I in which absorption is stochastically thick. The electron energies observed are close to the optimum condition, Eq. (6), in the text, which corresponds to the maximum of Fig. 2.

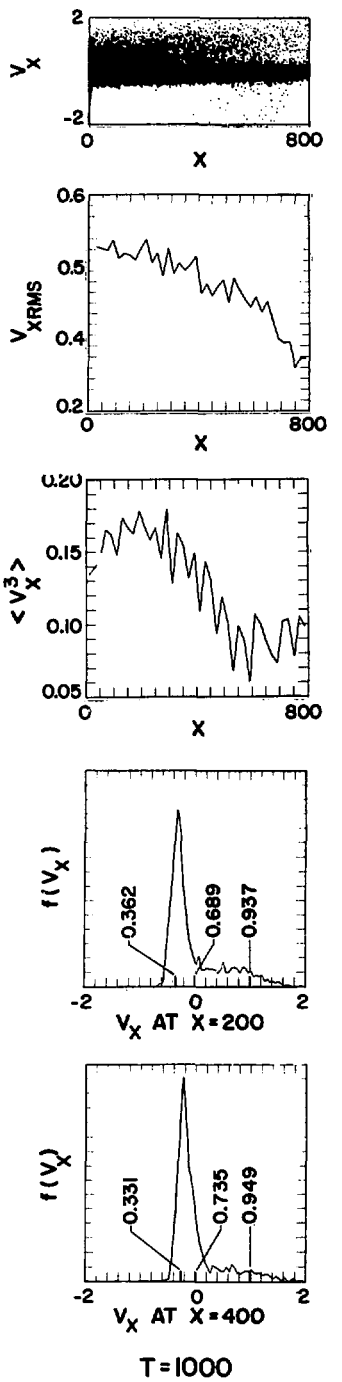

Fig. A-4. The same diagnostics as in Fig. A-3 at t = 1000 ω_{pe}^{-1}.

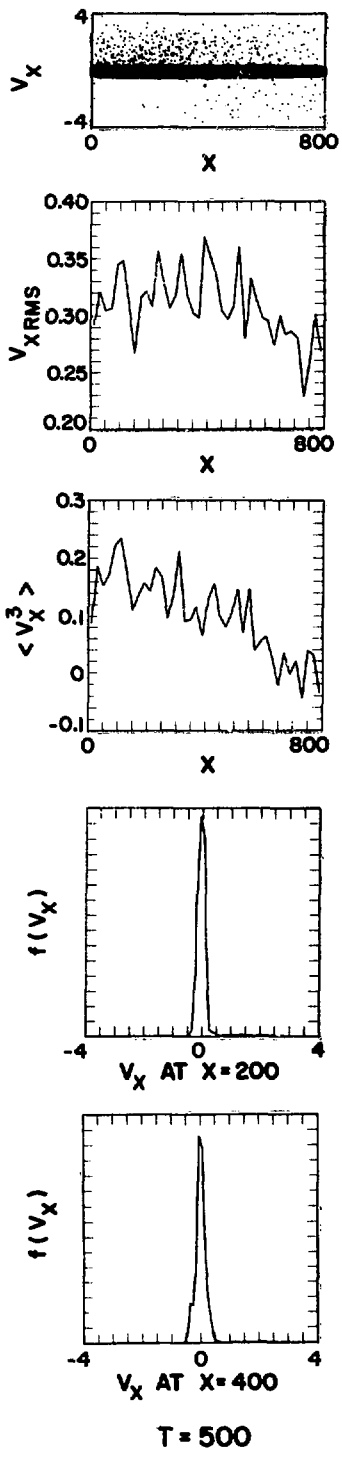

Fig. A-5. The same diagnostics at $t = 500\ \omega_{pe}^{-1}$ as in Fig. A-3 for the stochastically thin Case II, which corresponds to about the point $n_h/n = 0.1$ on Fig. Note the change of velocity scale from ±2.0 in Fig. A-3 to ±4.0 here.

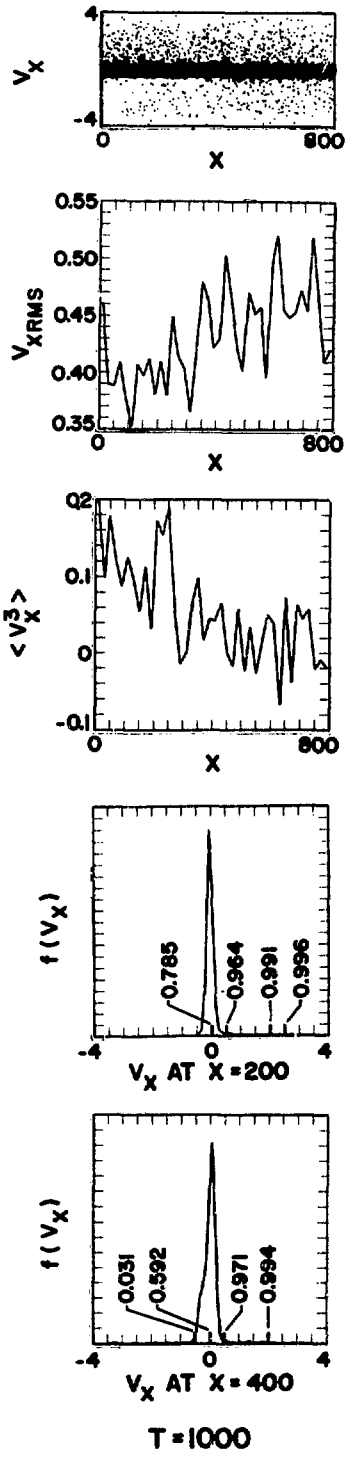

Fig. A-6. The same diagnostics as in Fig. A-5 at $t = 1000\ \omega_{pe}^{-1}$.

anisms equivalent for target heating purposes. Also, since many such absorption processes are quenched by a sufficiently large electron temperature in the absorption region, the absorption may regulate itself to that value of Q which is consistent with the quenching temperature through the thermal transport rate obtained here. In particular, as noted in the text, the temperatures required for a given thermal transport rate are much larger than the driven electron energies in the corresponding wave field and are, therefore, more difficult to achieve through absorption than if these temperatures were more nearly equal.

The collisionless transport process is illustrated by Figs. A-3 and A-4 which show numerical diagnostics at t = 500 and 1000 respectively. From top to botton these diagnostics are the phase space electron plot (showing only 1 of 5 of the total simulation particles), the mean value of v_x^3, $\langle v_x^3 \rangle$, as a function of position, $\langle (v_x - \langle v_x \rangle)^2 \rangle$, which we call Vrms, as a function of position, and the local velocity distribution function, $f(v_x)$, at x = 200 and 400. On these graphs of $f(v_x)$ marks and numbers have been added to the bottom which indicate the computed fraction of the particles represented which lie to the left of the selected velocities. These are added to help overcome difficulty with visual interpretation caused by the large difference in magnitude of the peaks and tails of these curves and by the fluctuations caused by taking a small local sample of particles. From the phase plots and graphs of $\langle v_x^3 \rangle$ and Vrms, it is seen that the energy is transported by a smooth, continuously rising flux of heated electrons with no dramatic front structure, and with $\langle v_x^3 \rangle$ rising in the back to the value 0.166 (some visual smoothing of noise is required here) required by the heating parameters. The leading edge of the electron flux is seen to move at almost the maximum electron velocity generated in the heating region. The flow is slowed slightly by the electrostatic turbulence caused by the counter streaming instability and by the gross electrostatic fields which develop to force reverse flow of the cold electrons and maintain charge neutrality. These electrostatic fields of course decelerate the less strongly heated electrons most and have the effect of filling in what would otherwise be a small gap in velocities between the heated electrons which leave the heating region with only positive velocities and the cold electrons which stream back into the heating region with relatively small but distinctly negative velocities. What happens is that as the flux of heated electrons progresses into the unheated plasma the electrostatic fields decelerate the slower electrons and turn them back toward the heating region, thus tending to fill in the gap and eliminating instability. This filling tends to flatten the velocity distribution toward the idealized form used in the text. However, as the heated electrons move into the higher density of the target, where n_h/n becomes much smaller and the collision frequency may approach or even exceed the plasma frequency, both the gross and turbulent electrostatic fields must be smaller and some of the two beam structure of the velocity distribution must reappear.

From the distribution function graphs in Figs. A-3 and A-4, and particularly the distribution at t = 1000 and x = 200, it can be seen that where the energy flux has established itself at its steady state value, the fraction of electrons in the tail, n_h/n, is about 0.30 ± 0.05, which brackets the optimum value of n_h/n in Fig. 2. The effective maximum velocity of the hot electrons, defined as v_h in the text, is about 1.5. This value of v_h, together with Q = 0.166 from above gives $Q/(nmv_h^3/2) = 4.9 \times 10^{-2}$, which is only a little below the maximum or optimum, value of this ratio obtained from the analytic model in the text. This simulation has shown then that stochastically thick absorption gives rise to electron transport with parameters close to those corresponding to the maximum of Fig. 2 in the text.

CASE II

This case is the same as Case I in all respects except that the maximum velocity increment in the heating process, δv_{max}, has been increased from 0.1 to 3.0, and the fraction of particles in the interval x = 0 to 10 that are incremented on each time step has been decreased from 1.0 to 1/900. These changes, which place Case II clearly into the stochastically thin heating region, just compensate so as to keep Q, and therefore $\langle v_x^3 \rangle$, the same as in

Case I. Figures A-5 and A-6 show the same diagnostics at t = 500 and 1000 as do A-3 and A-4 for Case I. Notice, however, that the velocity limits on the phase plots and distribution graphs have been increased from + 2 in Case I to + 4. The most obvious difference is that the energetic electron velocities are larger and, therefore, that the front of the profiles of $\langle v_x^3 \rangle$ and Vrms move more rapidly than in Case I. This is consistent with the same value of Q and $\langle v_x^3 \rangle$ behind the front because the specific heat of the energetic electrons is smaller in Case II, as reflected by the smaller values of Vrms. This in turn is a consequence of the smaller values of n_h/n, which can be seen from $f(v_x)$ at t = 1000 and x = 200 to be $n_h/n \simeq 0.04$, a value well to the low density side of the optimum of Fig. 2 in the text. From Fig. 2 the ratio $Q/(nmv_2^3/2)$ should be about 0.01, which indicates a value of v_h that is larger than the $v_h = 1.5$ in Case I by a factor of about 1.5, or $v_2 = 2.4$. This is consistent with $f(v_x)$ at t = 1000 and x = 200, and, therefore, supports the approximate validity of the analytic model for stochastically thin absorption.

The short wave length beam instability driven oscillations of the cold electrons are also seen here in Case II, as is the tendency of the high energy tail to flatten and fill in at lower velocities. In $f(v_x)$ at t = 1000 and x = 400 we also see a significant negative velocity tail of returning high energy electrons, as in the idealized distribution of Fig. 1c in the text.

REFERENCES

1. D. F. Dubois and M. V. Goldman, Phys. Rev. Lett. 14, 544 (1965); P. K. Kaw and J. M. Dawson, Phys. Fluids 12, 2586 (1969); J. P. Freidberg and B. M. Marder, Phys. Rev. A4, 1549 (1971). This is only a partial list.
2. J. P. Freidberg, R. W. Mitchell, R. L. Morse, and L. I. Rudsinski, Phys. Rev. Lett. 28, 795 (1972).
3. D. W. Forslund, J. Geophys. Res. 75, 17 (1970).
4. R. L. Morse and C. W. Nielson, Phys. Rev. Lett. 26, 3 (1971).
5. E. W. Weibel, Phys. Rev. Lett. 2, 83 (1959).
6. R. L. Morse and C. W. Nielson, Phys. Fluids 14, 830 (1971).
7. R. L. Morse and C. W. Nielson, Phys. Rev. Lett. 23, 1087 (1969).
8. R. L. Morse and C. W. Nielson, Phys. Fluids 12, 2418 (1969). See also R. L. Morse in "Methods in Computational Physics," edited by B. Alder, S. Fernbach and M. Rotenberg (Academic Press, New York, 1970), Vol. 9, p. 213.

EE/ml:537(300)